Scripta Materialia 108 (2015) 35–39

Contents lists available at ScienceDirect

Scripta Materialia

journal homepage: www.elsevier.com/locate/scriptamat

Strengthening high-stacking-fault-energy metals via parallelogram nanotwins

Yuefei Zhang [a,*], Jin Wang [a], Haiquan Shan [a], Kejie Zhao [b,*]

[a] Institute of Microstructure and Property of Advanced Materials, Beijing University of Technology, Beijing 100124, PR China
[b] School of Mechanical Engineering, Purdue University, West Lafayette, IN 47906, USA

ARTICLE INFO

Article history:
Received 19 March 2015
Revised 19 May 2015
Accepted 22 May 2015
Available online 15 June 2015

Keywords:
Nanotwins
Ni
Twin patterns
Electrodeposition
Parallelogram

ABSTRACT

Twins readily form during growth or deformation in metals of low stacking-fault energy. Fabrication of high-density growth nanotwins in high stacking-fault energy materials is technically challenging. We synthesize nanotwinned Ni foils with controlled twin patterns – pulsed electrodeposition produces conventional parallel nanotwins while direct current electrodeposition generates a new pattern of nanotwins in the parallelogram form. The parallelogram nanotwins confine dislocation motion in the cage of twin boundaries and lead to a superior strengthening effect in Ni.

Nanotwinned (NT) metals exhibit unique properties of ultrahigh mechanical strength, enhanced ductility, superior thermal stability, and excellent electrical conductivity [1]. The attractive physical properties stem from the nature of $\Sigma3\{111\}$ coherent twin boundaries (CTBs) and the characteristic size at nanoscale [2,3]. CTBs with reduced spacing lead to the strengthening effect that is analogy to the classical Hall–Petch behavior. Meanwhile, nanoscale twins enhance the deformation ductility by retaining ample room to accommodate the dislocation accumulation. In addition, a small fraction of $\Sigma3\{112\}$ incoherent twin boundaries (ITBs) often coexist with CTBs in nanotwinned materials [4,5]. Propagation of ITBs contributes additional ductility of NT metals under a field of stress [5]. Despite the attractive mechanical properties, prior studies on NT metals focused on materials of low stacking-fault energy (SFE) or a low ratio of the unstable twin-fault energy (γ_{utf}) to the unstable stacking-fault energy (γ_{usf}) [6]. For high-SFE metals, dislocations are the predominant carriers to mediate the plastic deformation, although twins are occasionally activated at extreme conditions such as at crack tips, during high-pressure torsion or ball milling, and in deformed nanocrystalline grains [7–10]. Conventional processes to fabricate high-density growth nanotwins in low-SFE metals include electrodeposition, magnetron sputtering, electron-beam evaporation, plastic deformation, and phase transformation [11–14]. Synthesis of high-density growth twins in metals of high SFE has been extremely challenging. A few efforts were made to fabricate growth nanotwins in Ni/Cu multilayers or by adding alloying elements in the plating bath to facilitate the nucleation of twin seeds [15,16]. Successful synthesis of high-density nanotwins in pure metals of high-SFE, however, is rare, which limits the utilization of nanotwins to strengthen a broad variety of engineering materials [11,17].

The primary scope of this study is to report a feasible route to synthesize bulk Ni (SFE 125 mJ/m^2) with a high density of nanoscale twins by electrodeposition. Twin orientations can be controlled by varying the input current – pulsed electrodeposition fabricates Ni samples with nanotwins parallel to each other in grains, while direct current (DC) electrodeposition leads to a regular two-dimensional pattern that two sets of parallel twins constitute parallelograms. The average grain size and twin thickness can be well controlled by modifying a series of electrodeposition parameters. The parallelogram nanotwins, distinct from the conventional parallel twins in low-SFE materials, lead to ultrahigh mechanical strength and tensile ductility. The enhanced mechanical properties of parallelogram NT samples are attributed to the confinement effect for dislocation motion thus a larger capacity of dislocation storage and accumulation.

Table S1 summarizes the experimental conditions. Each parameter is varied separately in a given range to test the individual effect on the microstructure of as-deposited samples. The quantitative effects of the bath temperature, current density, Ni^{2+} concentration, and ratio of current on-time and off-time (T_{on}/T_{off}) on the average grain size, twin thickness, and twin length are illustrated

* Corresponding authors.
E-mail addresses: yfzhang@bjut.edu.cn (Y. Zhang), kjzhao@purdue.edu (K. Zhao).

http://dx.doi.org/10.1016/j.scriptamat.2015.05.039
1359-6462/

in the Tables S2–S5. Overall, the increase of the above experimental controls results in a decrease of the average grain size and an increase of the twin density (Table S6). The explicit mechanism of nanotwinned Ni fabricated by the simple conditions of electrodeposition remains unclear at this writing due to the complex nature of electrochemical processes. Nevertheless, we aspire to disclose the experimental details that repeatedly produce the intriguing nanotwin patterns as summarized in the Tables S1–S6.

The as-deposited Ni foils have in-plane dimensions of 30 mm by 30 mm and a thickness of 30 μm with a uniform columnar-grained microstructure and high purity (Figs. S1 and S2). Here we will focus on the characterization of the parallelogram nanotwins. Information on parallel twins is included in the Supplementary materials. Fig. 1a shows a transmission electron microscopy (TEM) image on the morphology of parallelogram twins embedded in submicron grains. The grain sizes are between 400 nm and 800 nm. Each grain is divided into parallelograms by a high density of growth twins. Measurements of the twin thickness along the [1 1 0] orientation show a wide distribution ranging from several nanometers to about 120 nm. High-resolution TEM (HRTEM) observations illustrate rich microstructural features. Multiple-fold twin boundaries exist at the junctions of parallelogram twins to fulfill the geometric compatibility (Fig. 2c) [18–20]. A mismatch angle presents at the junction of multiple-fold twin boundaries. In fivefold twins, for instance, the angle between two neighboring {1 1 1} planes is 1.47° smaller than that required to perfectly cover one fifth of a circle. Such a mismatch gap is accommodated by stretching and broadening individual twin boundaries, which may act as a source of stress concentration and dislocation nucleation. Multiple-fold twin boundaries also connect with grain boundaries (GBs) and form a complex twin network structure. CTBs and ITBs also coexist (Fig. 2d). The densities of CTBs and ITBs in parallelogram nanotwins are 4.5×10^{14} m^{-2} and 5.8×10^{13} m^{-2}, respectively. The microstructural features of parallel nanotwins are shown in Fig. S3. It is noteworthy that the densities of CTBs and ITBs in parallelogram NT samples are markedly larger than their counterparts in parallel nanotwins -2.9×10^{14} m^{-2} for CTBs and 1.9×10^{13} m^{-2} for ITBs.

Thermal stability of the growth nanotwins in as-deposited Ni foils is characterized by isothermal annealing. Detailed experimental procedure is shown in the Supplementary materials. *In situ* TEM observations of the microstructural evolution of parallelogram twins annealed at 100 °C, 200 °C, 300 °C, 400 °C, 500 °C, and 600 °C are shown in Fig. 2. Detwinning is observed in the samples annealed above 400 °C.

Tensile tests of NT foils are performed at a nominal strain rate of 10^{-4} s^{-1} at ambient temperature. Fig. 3 shows the high strength of parallelogram NT samples in comparison with that of parallel NT samples, a coarse-grained polycrystalline Ni sample, and a nanocrystalline Ni sample. The microstructures of nanocrystalline and coarse-grained Ni and grain size distributions are shown in Fig. S4. The parallelogram NT Ni samples also show considerable tensile ductility, with an elongation-to-failure strain of 6.5%, which is much higher than the nanocrystalline specimen. A slight strain hardening appears in the plot of engineering stress versus engineering strain during the major stage of plastic deformation. Converting the plot to true stress versus true strain, the work hardening would become more prominent, indicative of dislocation

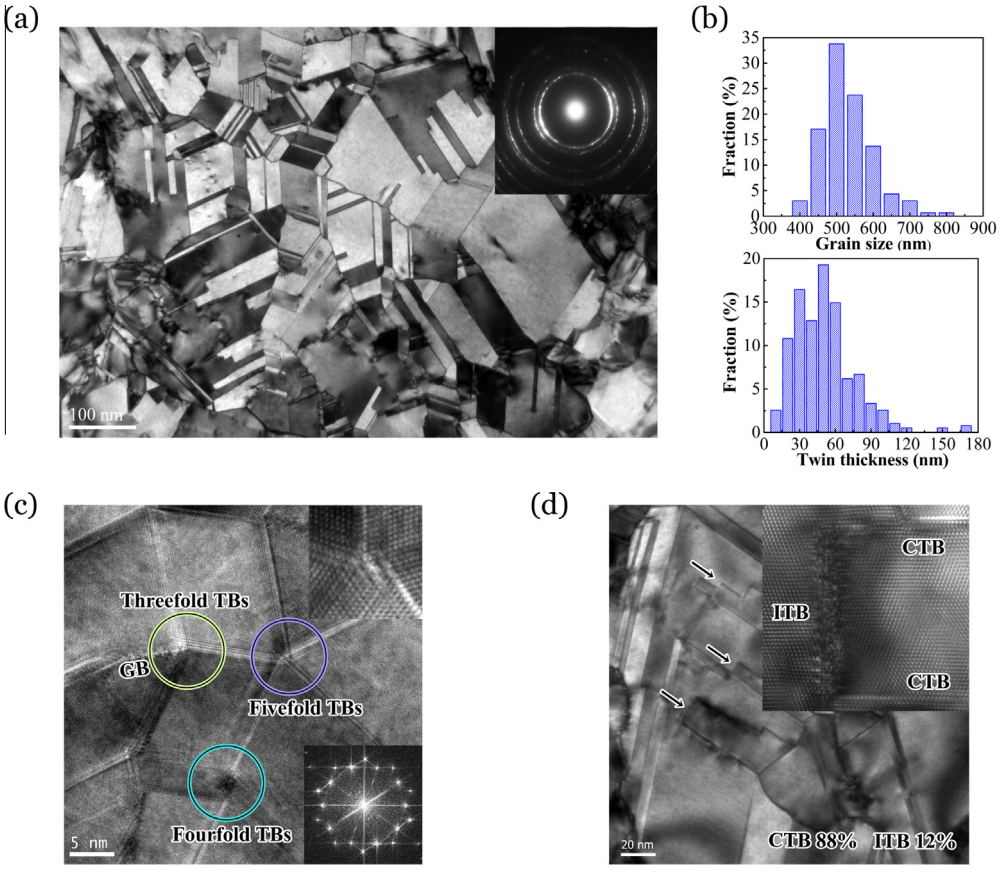

Fig. 1. (a) The bright-field TEM image shows high-density parallelogram nanotwins in a Ni sample synthesized by DC electrodeposition. Electron diffraction pattern (inset) shows roughly equiaxed submicron grains with random orientations. (b) Statistical distributions of the grain size and the twin thickness. (c) Multiple-fold twin boundaries exist at the junctions of parallelogram twins to fulfill the geometric compatibility. The fivefold TBs are broadened to accommodate the mismatch angle as shown in the HRTEM image (inset). (d) CTBs and ITBs coexist. The percentage of CTBs and ITBs are 88% and 12% respectively.

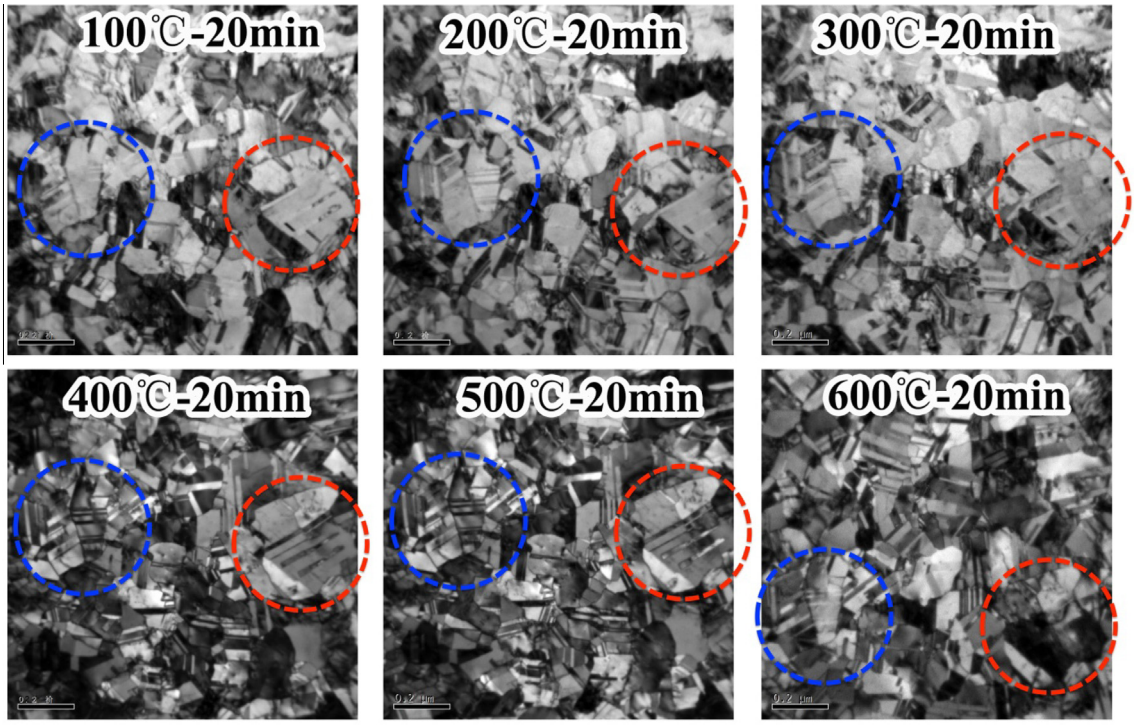

Fig. 2. Thermal stability of the growth nanotwins in as-deposited Ni foils. *In situ* TEM observations of the microstructure of parallelogram twins isothermally annealed at 100 °C, 200 °C, 300 °C, 400 °C, 500 °C, and 600 °C respectively. Detwinning is observed in the circled areas annealed above 400 °C.

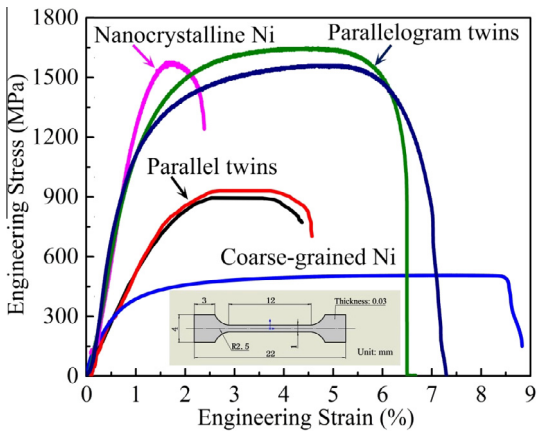

Fig. 3. Stress–strain curves for the as-deposited Ni samples with parallel and parallelogram nanotwins (with typical twin thickness of 30 nm and 50 nm respectively, the average of grain sizes are both in between 300 and 500 nm) in comparison with that for a coarse-grained polycrystalline Ni sample (with an average grain size of ca. 400 nm) and a nanocrystalline Ni sample (with an average grain size of ca. 20 nm). Each type of nanotwinned Ni is tested with two samples. The inset sketches the geometry of the samples.

accumulation before failure [21]. Necking and shear cracking occur upon tensile fracture. The fracture surfaces (Fig. S5) demonstrate dimpled rupture and microvoid coalescence. The dimple sizes are between a few hundred nanometers and several micrometers with an average value of a few times of the average grain size. It is noteworthy that by varying the grain size and twin thickness it may induce size-dependent deformation behaviors and failure mechanisms. Such size effects would be intriguing for further systematic studies [22]. The difference in the elastic modulus between parallel twinned Ni and those with parallelogram nanotwins is primarily due to the different current densities in the fabrication of the two sets of samples. The tested samples with parallelogram twins were fabricated at a current density of 15 A/dm^2, while a current density of 36 A/dm^2 was provided for the parallel twin samples. The high current density generally leads to a less dense structure with lower elastic modulus [23–25].

The strengthening mechanism by means of nanotwins in metals is generally attributed to the interactions between glide dislocations and twin boundaries. CTBs act as a strong barrier for dislocation motion leading to a strengthening behavior analogous to that of conventional GBs. HRTEM images in Fig. S6 show that high-density of dislocations pile-up at CTBs and transmit across the twin boundaries. The interactions between dislocations with CTBs generate a large number of stacking faults. The segregation of dislocations distorts the twin boundaries. The reactions between dislocations in face-centered cubic metals and twin boundaries generate glissile Shockley partial dislocations (SPDs) and sessile Frank dislocations (FDs). The glissile partial dislocations may propagate across the twin boundaries, while the sessile dislocations are left at the boundaries and result in a loss of coherency of CTBs [26]. Nevertheless, other dislocation reactions cannot be excluded and may also be operative in the strengthening mechanism [27,28]. Dislocations nucleated at various sites of structural defects, primarily at GBs and intersections with twin boundaries, slip along the twin planes. The successive motion of glissile dislocations leads to the migration of CTBs that mediates the plastic flow of NT Ni, Fig. S6b [29]. In addition, ITBs are another important carrier of twining plasticity. ITBs are highly mobile, Fig. S6c, which requires a much smaller resolved shear stress than that required to emit twinning partial dislocations from GBs with perfect CTBs [4]. Detwinning is accompanied with the migration of ITBs via the collective slip of multiple twin dislocations, Fig. S6d [30]. The deformation mechanisms of NT Ni observed in our experiments share much similarity with that of NT Cu which has been intensively studied. This observation might be roughly understood that both Ni and Cu have low ratios of stacking fault energy (γ_{sf}) to γ_{usf} and $\gamma_{usf}/\gamma_{utf}$, such that partial dislocations dominantly mediate

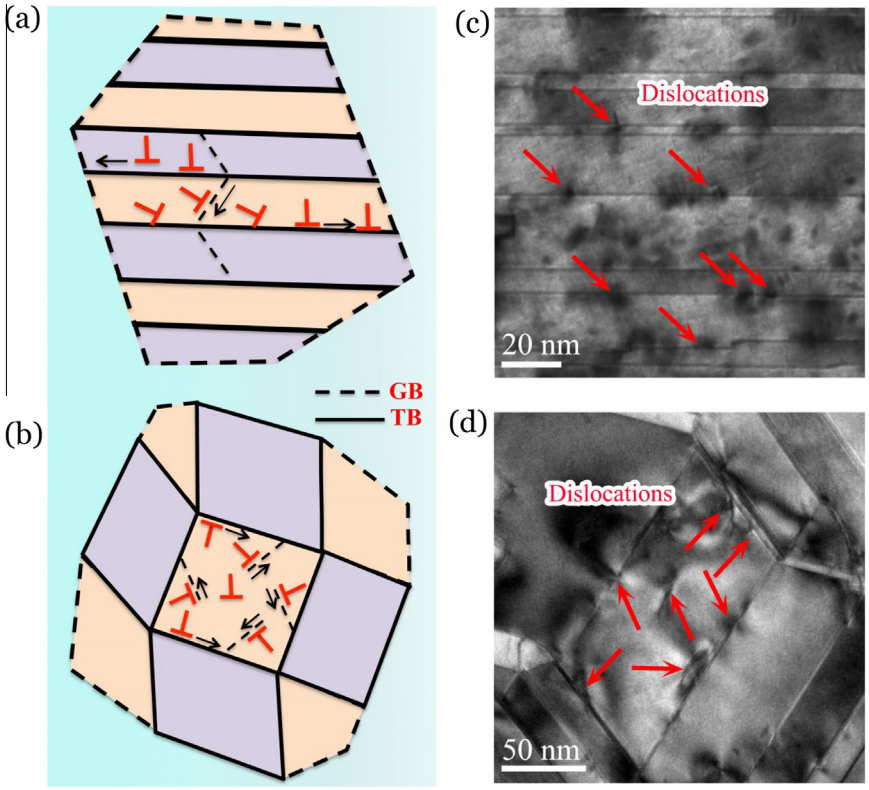

Fig. 4. Dislocation activities in parallel and parallelogram nanotwinned Ni after applying a tensile strain of ~5%. (a and c) For parallel nanotwins, dislocations are primarily located at the twin boundaries and few are seen inside lamellar layers. (b and d) For parallelogram nanotwins, dislocations are confined in the cage of twin boundaries and are observed in both the vicinity and interior of twin boundaries.

plasticity in both materials. Detailed atomistic pictures in high-SFE metals warrant further careful studies [12].

Despite the common deformation mechanisms in the parallel and parallelogram NT Ni, the NT patterns interplay with dislocations in different manners. For parallel nanotwins, dislocations are confined only by the thickness of twin lamellae while a sufficient free path is maintained for dislocation slip along the length orientation, Fig. 4a. In contrast, dislocations are confined in the cage of parallelogram twin boundaries. Such confined spaces may be effectively regarded as sub-equiaxed-grains, Fig. 4b. The reduced size results in more accumulative dislocations at the twin boundaries and thereby a better strengthening effect of parallelogram nanotwins. It is confirmed by our observations that dislocations are located in both the vicinity and interior of twin boundaries for the parallelogram twins, while dislocations in parallel twins primarily pile-up near the twin boundaries and few are seen inside the twin lamellae, Fig. 4c and d. Furthermore, the densities of CTBs and ITBs in the parallelogram form are inherently larger than that in the parallel twin samples. It is conceivable that the dislocation density in parallelogram nanotwins is much larger than the counterparts of parallel twins upon deformation. We may estimate the material strength following the Taylor-type relationship, $\sigma_{\text{flow}} \sim \sqrt{\rho}$, where ρ is the dislocation density. A larger capacity for dislocation storage and accumulation renders higher mechanical strength and extended ductility in parallelogram nanotwins. Beyond the Taylor-type strengthening argument, it is also plausible that dislocations from multiple slip systems intersect at twin boundaries in the parallelogram nanotwins that abundant Lomer–Cottrell (L–C) locks may form to enhance the work hardening capability. The L–C locks were recently observed within grains and at twin boundaries in nanocrystalline Ni [31].

In summary, we synthesized nanotwinned Ni foils with controlled spacing and pattern through conventional electrodeposition. The parallelogram nanotwins are distinct from the parallel twins that are commonly observed in low-SFE metals. Such a pattern confines dislocation motion in the interior space of twin boundaries, and may inspire a new strategy of designing high-strength metals via patterned nanotwins.

Acknowledgments

Y.Z. acknowledges the National Natural Science funded project (11374027) and Special Projects for Development of National Major Scientific Instruments and Equipment (2012YQ03007508). The research project is supported by the start-up funds at Purdue University. K.Z. acknowledges helpful discussions with Dr. Xiangdong Ding, Dr. Shaoxing Qu, and Dr. Jian Wang. K.Z. is grateful for the support of Haythornthwaite Foundation Initiation Grant from American Society of Mechanical Engineering.

Appendix A. Supplementary data

Supplementary data associated with this article can be found, in the online version, at http://dx.doi.org/10.1016/j.scriptamat.2015.05.039.

References

[1] Y. Lu, X. Shen, L. Chen, K. Qian Lu, Science 304 (2004) 422–426.
[2] K. Lu, L. Lu, S. Suresh, Science 324 (2009) 349–352.
[3] L. Lu, X. Chen, X. Huang, K. Lu, Science 323 (2009) 607–610.
[4] Y.M. Wang, F. Sansoz, T. LaGrange, R.T. Ott, J. Marian, T.W. Barbee Jr., A.V. Hamza, Nat. Mater. 12 (2013) 697–702.

[5] J. Wang, N. Li, O. Anderoglu, X. Zhang, A. Misra, J. Huang, J. Hirth, Acta Mater. 58 (2010) 2262–2270.
[6] H. Van Swygenhoven, P. Derlet, A. Frøseth, Nat. Mater. 3 (2004) 399–403.
[7] H. Zhou, S. Qu, W. Yang, Model. Simul. Mater. Sci. Eng. 18 (2010) 065002.
[8] J. Huang, Y. Wu, H. Ye, Acta Mater. 44 (1996) 1211–1221.
[9] X. Wu, Y. Zhu, M. Chen, E. Ma, Scripta Mater. 54 (2006) 1685–1690.
[10] X. Liao, F. Zhou, E. Lavernia, D. He, Y. Zhu, Appl. Phys. Lett. 83 (2003) 5062–5064.
[11] H. Idrissi, B. Wang, M.S. Colla, J.P. Raskin, D. Schryvers, T. Pardoen, Adv. Mater. 23 (2011) 2119–2122.
[12] D. Bufford, Y. Liu, J. Wang, H. Wang, X. Zhang, Nat. Commun. 5 (2014) 4864.
[13] D. Bufford, H. Wang, X. Zhang, Acta Mater. 59 (2011) 93–101.
[14] V. Yamakov, D. Wolf, S. Phillpot, H. Gleiter, Acta Mater. 50 (2002) 5005–5020.
[15] Y. Liu, D. Bufford, S. Rios, H. Wang, J. Chen, J. Zhang, X. Zhang, J. Appl. Phys. 111 (2012) 073526.
[16] G. Lucadamo, D. Medlin, N. Yang, J. Kelly, A. Talin, Philos. Mag. 85 (2005) 2549–2560.
[17] D. Bufford, Y. Liu, Y. Zhu, Z. Bi, Q. Jia, H. Wang, X. Zhang, Mater. Res. Lett. 1 (2013) 51–60.
[18] X. Liao, J. Huang, Y. Zhu, F. Zhou, E. Lavernia, Philos. Mag. 83 (2003) 3065–3075.
[19] H. Chen, Y. Gao, H. Zhang, L. Liu, H. Yu, H. Tian, S. Xie, J. Li, J. Phys. Chem. B 108 (2004) 12038–12043.
[20] Y. Zhu, X. Liao, R. Valiev, Appl. Phys. Lett. 86 (2005) 103112.
[21] Y. Shen, L. Lu, Q. Lu, Z. Jin, K. Lu, Scripta Mater. 52 (2005) 989–994.
[22] Z. Wu, Y. Zhang, M. Jhon, D. Srolovitz, Acta Mater. 61 (2013) 5807–5820.
[23] J. Luo, M. Pritschow, A. Flewitt, S. Spearing, N. Fleck, W. Milne, J. Electrochem. Soc. 153 (2006) D155–D161.
[24] T. Fritz, M. Griepentrog, W. Mokwa, U. Schnakenberg, Electrochim. Acta 48 (2003) 3029–3035.
[25] Y. Woo, S.-H. Kim, J. Mech. Sci. Technol. 25 (2011) 1017–1022.
[26] B. Wang, H. Idrissi, M. Galceran, M.-S. Colla, S. Turner, S. Hui, J.-P. Raskin, T. Pardoen, S. Godet, D. Schryvers, Int. J. Plast. 37 (2012) 140–156.
[27] Z. Wu, Y. Zhang, D. Srolovitz, Acta Mater. 57 (2009) 4508–4518.
[28] D. Jang, X. Li, H. Gao, J.R. Greer, Nat. Nanotechnol. 7 (2012) 594–601.
[29] Z. You, X. Li, L. Gui, Q. Lu, T. Zhu, H. Gao, L. Lu, Acta Mater. 61 (2013) 217–227.
[30] J. Wang, A. Misra, J. Hirth, Phys. Rev. B 83 (2011) 064106.
[31] J.H. Lee, T.B. Holland, A.K. Mukherjee, X. Zhang, H. Wang, Sci. Rep. 3 (2013) 1061.